General Disclaimer

One or more of the Following Statements may affect this Document

- This document has been reproduced from the best copy furnished by the organizational source. It is being released in the interest of making available as much information as possible.

- This document may contain data, which exceeds the sheet parameters. It was furnished in this condition by the organizational source and is the best copy available.

- This document may contain tone-on-tone or color graphs, charts and/or pictures, which have been reproduced in black and white.

- This document is paginated as submitted by the original source.

- Portions of this document are not fully legible due to the historical nature of some of the material. However, it is the best reproduction available from the original submission.

Non-Newtonian Fluid Model Incorporated into Elastohydrodynamic Lubrication of Rectangular Contacts

Bo O. Jacobson and Bernard J. Hamrock
Lewis Research Center
Cleveland, Ohio

NASA

NON-NEWTONIAN FLUID MODEL INCORPORATED INTO ELASTOHYDRODYNAMIC
LUBRICATION OF RECTANGULAR CONTACTS

Bo O. Jacobson

University of Luleå

Luleå, Sweden

and

Bernard J. Hamrock

National Aeronautics and Space Administration

Lewis Research Center

Cleveland, Ohio 44135

SUMMARY

A procedure is outlined for the numerical solution of the complete elastohydrodynamic lubrication of rectangular contacts incorporating a non-Newtonian fluid model. The approach uses a Newtonian model as long as the shear stress is less than a limiting shear stress. If the shear stress exceeds the limiting value, the shear stress is set equal to the limiting value. The numerical solution requires the coupled solution of the pressure, film shape, and fluid rheology equations from the inlet to the outlet. Isothermal and no-side-leakage assumptions were imposed in the analysis.

The influence of dimensionless speed U, load W, materials G, and sliding velocity U^* and limiting-shear-strength proportionality constant γ on dimensionless minimum film thickness H_{min} was investigated. Fourteen cases were used in obtaining the minimum-film-thickness equation for an elastohydrodynamically lubricated rectangular contact incorporating a non-Newtonian fluid model

$$\bar{H}_{min} = \bar{H}_{min,N}\left\{\exp\left[-4.09\times10^{-9}(U^*)^{0.60}U^{0.23}(WG^2)^{3.85} + 2.06(\gamma - 0.07)\right] + U^*\right\}^{0.71}(1 - U^*)^{0.71}$$

where

$$\bar{H}_{min,N} = 3.07 \ U^{0.71} G^{0.57} W^{-0.11}$$

Computer plots are also presented that indicate in detail pressure distribution, film shape, shear stress at the surfaces, and flow throughout the conjunction.

INTRODUCTION

To obtain a better understanding of the failure mechanism in machine elements, the next generation of elastohydrodynamic lubrication analysis should incorporate such effects as

(a) Non-Newtonian fluid

(b) Surface roughness

(c) Temperature

Although a Newtonian solution for elliptical contacts had been obtained by Hamrock and Dowson (1981), it was felt that a rectangular or line-contact analysis should be used to incorporate these effects because of their added complexity. A rectangular or line-contact analysis was performed by Hamrock and Jacobson (1982). The analysis required the simultaneous solution of the elasticity and Reynolds equations. The equations were coupled from the inlet to the outlet assuming isothermal conditions and no side leakage. The results from Hamrock and Jacobson (1982) are the foundation for the more complicated analysis incorporating non-Newtonian fluid, surface roughness, and temperature. When considering these effects, the initial pressure profiles are those obtained from the authors' earlier work.

The present paper considers incorporating a non-Newtonian fluid model into the theory of elastohydrodynamic lubrication of rectangular contacts. The geometry of the problem is a roller, rolling and sliding against a plate,

2

where the roller length is large as compared with the radius. The lubricant in an elastohydrodynamic conjunction experiences rapid and very large pressure variations, a rapid transit time, possible large temperature changes, and particularly in sliding contacts, high shear rates. The great severity of these conditions has called into question the normal assumption of New- tonian behavior. The approach to be used in this paper is to redefine the pressure and mass flow rate equations depending on how the values of shear stress at the surfaces compare with the limiting shear stress. The limiting shear expression used is a semiempirical linear function of pressure.

Gacim and Winer (1981) used a non-Newtonian fluid rheological model in their elastohydrodynamic lubrication studies. Some limitations of this work are listed below:

(1) The analysis assumes a non-Newtonian fluid model for the entire conjuction including the inlet region. The present paper uses a non-Newtonian fluid model only when the shear stress at the surfaces exceeds the limiting shear stress.

(2) The Gacim and Winer analysis relies on using a Grubin type of solution rather than employing a complete solution of the Reynolds, rheology, and film shape equations as is used in the present paper.

(3) The Gacim and Winer paper assumes that the limiting shear stress is zero when the fluid pressure is zero. The present paper assumes that the limiting shear stress is equal to an initial shear strength when the pressure is zero.

Figure 1 shows the effect of shear stress on shear strain rate for the present model and that of a Newtonian fluid. From this figure it is observed that, in the present model, if the Newtonian shear stress exceeds the limiting shear stress, the shear stress is set equal to the limiting shear stress.

3

The fluid model is Newtonian except when the shear stress reaches the shear strength value. At that point, slippage occurs and the shear stress is equal to the shear strength.

Besides the dimensionless load, speed, and materials parameters that were found to have an influence on film thickness in the authors' earlier paper (Hamrock and Jacobson, 1982), when non-Newtonian effects are considered, two additional parameters were found to influence the minimum film thickness, namely:

(1) Sliding velocity

(2) Limiting-shear-strength proportionality constant

Fourteen cases were used in obtaining a fully flooded film thickness equation when considering non-Newtonian effects of the liquid. Besides the film thickness calculations that were made, calculations of the force components, shear forces, coefficient of friction, and center of pressure were also performed. Computer plots are presented that indicate pressure distribution, lubricant film shape, flow, and shear stresses within the conjunction.

SYMBOLS

B	$1/n$
b	semiwidth of Hertzian contact, $R\sqrt{8W/\pi}$, m
$\bar{b}$	b/n, m
E	modulus of elasticity, N/m^2
E'	effective elastic modulus, $2/[(1 - v_a^2)/E_a + (1 - v_b^2)/E_b]$, N/m^2
$\bar{f}$	dimensionless shear force
f	shear force per unit length, N/m
G	dimensionless materials parameter, $\alpha E'$
H	dimensionless film thickness, h/R
H_{min}	dimensionless minimum film thickness, h_{min}/R

$\overline{H}_{min}$	dimensionless minimum film thickness obtained from least-squares fit of data
$\overline{H}_{min,N}$	dimensionless minimum film thickness obtained from least-squares fit of data while assuming a Newtonian fluid model
h	film thickness, m
h_{min}	minimum film thickness, m
m	dimensionless distance from inlet to the center of Hertzian contact
n	number of nodes in semiaxis of contact
P	dimensionless pressure, p/E'
p	pressure, N/m^2
Q	dimensionless mass flow per unit length, $q/\rho_0 u_s R$
q	mass flow per unit length, $kg/(s \cdot m)$
R	effective radius in x direction, m
r	curvature radius, m
S	geometrical separation, m
U	dimensionless speed parameter, $\eta_0 u_s/E'R$
U	dimensionless velocity, u/u_s
U^*	dimensionless sliding velocity, u_d/u_s
u	velocity in direction of motion, m/s
u_d	velocity difference, $(u_a - u_b)/2$, m/s
u_s	velocity sum, $(u_a + u_b)/2$, m/s
V_1	$(\overline{H}_{min} - H_{min})100/H_{min}$
V_3	$(\overline{\mu} - \mu)\,100/\mu$
W	dimensionless load parameter, $w_z/E'R$
w_z	load per unit length, N/m
X	dimensionless coordinate, x/b

x	coordinate in direction of motion, m	
Z	dimensionless coordinate in direction of film, z/h	
z	coordinate in direction of film thickness, m	
α	pressure-viscosity coefficient of lubricant, m^2/N	
γ	limiting-shear-strength proportionality constant	
δ	elastic deformation, m	
ϵ	coefficient of determination	
η	absolute viscosity at gage pressure, $N\ s/m^2$	
$\bar{\eta}$	dimensionless viscosity, η/η_0	
η_0	viscosity at atmospheric pressure, $N\ s/m^2$	
μ	coefficient of friction	
ν	Poisson's ratio	
ρ	lubricant density, kg/m^3	
$\bar{\rho}$	dimensionless density, ρ/ρ_0	
ρ_0	density at atmospheric pressure, kg/m^3	
τ	shear stress, N/m^2	
$\bar{\tau}$	dimensionless shear stress, τ/E'	
τ	shear stress ratio, τ/τ_L	
τ_L	limiting shear stress, N/m^2	
$\bar{\tau}_L$	dimensionless limiting shear stress, τ_L/E'	
$\bar{\tau}_0$	dimensionless initial shear stress constant	

Subscripts:

a	solid a
b	solid b
x	coordinate in direction of motion
z	coordinate in direction of film thickness

THEORY

The non-Newtonian approach will be to consider the flow conditions at the surfaces. The flow has two components, the flow due to velocity (Couette) and the flow due to the pressure gradient (Poiseuille).

In figure 2 we attempt to explain the velocity of the fluid for the five distinct zones that might exist in an elastohydrodynamic conjunction when non-Newtonian effects of the lubricant are considered. In each zone the velocity of the top surface is greater than that of the bottom surface. To better indicate the difference between the zones, values of u_a and u_b will be kept constant for each zone. In figure 2(a), zone 0, the normal Newtonian zone, the shear stresses at the surfaces are less than the limiting shear stress, and no slippage of the fluid at the surfaces occurs. In figure 2(a), zone 1, the Newtonian shear stress at the top surface is larger than the limiting shear stress and slippage occurs at the top (faster) surface. In figure 2(a), zone 3, the shear stresses at both the top and bottom surfaces are outside the limiting range ($\bar{\tau}_a < -\bar{\tau}_L$ and $\bar{\tau}_b > \bar{\tau}_L$) and slippage occurs at both surfaces, but the slippage velocity is less than the velocity at the surfaces. In figure 2(b), zone 2, the Newtonian shear stress at the bottom surface is larger than the limiting shear stress, and slippage occurs at the bottom (slower) surface. In figure 2(b), zone 4, the same sort of situation is present as in zone 3 with the exception that the fluid slippage is greater than the surface velocity.

The relevant equations for the five distinct zones that can occur in an elastohydrodynamic lubrication contact when non-Newtonian effects are considered are developed next. Before we define these relevant equations for the

7

five zones, we need to define the dimensionless limiting shear strength. For most materials the shear strength varies linearly with pressure over wide pressure ranges, and there normally is a certain shear strength even at zero pressure. It is written as

$$\bar{\tau}_L = \bar{\tau}_0 + \gamma P \tag{1}$$

where

$\bar{\tau}_0$ dimensionless initial shear strength

γ limiting-shear-strength proportionality constant

Jacobson (1970) found values of $\bar{\tau}_0$ for a range of fluids to be between 1×10^{-5} and 1×10^{-4}. For the results given in that paper $\bar{\tau}_0$ was assumed to be 9×10^{-5}. Bair and Winer (1979) found γ to be between 0.05 and 0.10 for a complete range of natural and synthetic lubricating oils. Tevaarwerk (1976) used similar values of γ in his traction studies. In the present paper we consider a range of γ between 0.04 and 0.10.

Zone 0

The Newtonian model gives $\bar{\tau}_a < \bar{\tau}_L$ and $\bar{\tau}_b < \bar{\tau}_L$. In this zone the rheological model is a Newtonian fluid and no slippage occurs at either surface. The velocity distribution across the lubricant film for this situation is depicted in figures 2(a) and (b), zone 0. The velocity, the velocity gradient across the film, and the shear stress at the surfaces can be written directly from Hamrock and Dowson (1981) as

$$u = \frac{(z^2 - zh)}{2\eta} \frac{dp}{dx} + \frac{u_b(h - z)}{h} + \frac{u_a z}{h}$$

(2)

$$\frac{du}{dz} = \frac{(2z - h)}{2\eta} \frac{dp}{dx} + \frac{u_a - u_b}{h}$$

(3)

$$\tau_b = (\tau)_{z=0} = \eta \left(\frac{du}{dz}\right)_{z=0} = -\frac{h}{2}\frac{dp}{dx} + \frac{(u_a - u_b)\eta}{h}$$

(4)

$$\tau_a = (\tau)_{z=h} = \eta \left(\frac{du}{dz}\right)_{z=h} = \frac{h}{2}\frac{dp}{dx} + \frac{(u_a - u_b)\eta}{h}$$

(5)

Letting

$$X = \frac{x}{b}, \quad \frac{b}{R} = \sqrt{\frac{8W}{\pi}}, \quad \bar{\rho} = \frac{\rho}{\rho_0}, \quad \bar{\eta} = \frac{\eta}{\eta_0}, \quad H = \frac{h}{R}, \quad \frac{1}{R} = \frac{1}{r_a} + \frac{1}{r_b}, \quad G = \alpha E',$$

$$E' = \frac{2}{\dfrac{1 - v_a^2}{E_a} + \dfrac{1 - v_b^2}{E_b}}, \quad U = \frac{\eta_0 u_s}{E'R}, \quad u_s = \frac{u_a + u_b}{2}, \quad u_d = \frac{u_a - u_b}{2}, \quad \hat{U} = \frac{u}{u_s},$$

$$Z = \frac{z}{h}, \quad W = \frac{w_z}{E'R}, \quad U^* = \frac{u_d}{u_s} = \frac{u_a - u_b}{u_a + u_b}, \quad P = \frac{p}{E'}, \quad \bar{\tau}_b = \frac{\tau_b}{E'}, \quad \bar{\tau}_a = \frac{\tau_a}{E'}$$

(6)

equations (2) to (5) can be written in dimensionless form as

$$\hat{U} = 1 - U^*(1 - 2Z) + \frac{H^2}{4\bar{\eta}U} \sqrt{\frac{\pi}{2W}} Z(Z - 1)\frac{dP}{dX}$$

(7)

$$\frac{d\hat{U}}{dZ} = 2U^* + \frac{H^2}{4\bar{\eta}U} \sqrt{\frac{\pi}{2W}} (2Z - 1)\frac{dP}{dX}$$

(8)

$$\bar{\tau}_b = \frac{2UU^*\bar{\eta}}{H} - \frac{H}{4} \sqrt{\frac{\pi}{2W}} \frac{dP}{dX}$$

(9)

$$\bar{\tau}_a = \frac{2UU^*\bar{\eta}}{H} + \frac{H}{4} \sqrt{\frac{\pi}{2W}} \frac{dP}{dX}$$

(10)

Since this is zone 0, the Newtonian model gives $\bar{\tau}_a < \bar{\tau}_L$ and $\bar{\tau}_b < \bar{\tau}_L$. The dimensionless mass flow per unit length and its gradient set equal to zero give

$$Q = \frac{q}{\rho_0 u_s R} = \bar{\rho}H \int_0^1 \hat{U} \, dZ = \bar{\rho}H \left(1 - \frac{H^2}{24\bar{\eta}U} \sqrt{\frac{\pi}{2W}} \frac{dP}{dX}\right)$$ (11)

$dQ/dX = 0$ gives

$$\frac{d}{dX}\left(\frac{\bar{\rho}H^3}{\bar{\eta}} \frac{dP}{dX}\right) = 24U \sqrt{\frac{2W}{\pi}} \frac{d}{dX}(\bar{\rho}H)$$ (12)

The second term on the right side of equation (11) is the Poiseuille or pressure term. For a Newtonian fluid equation (12) is the familiar Reynolds equation when side leakage is neglected. This equation will be referred to as the pressure equation since it will change for the respective zones.

Zone 1

The Newtonian model for zone 1 gives $\left|\bar{\tau}_a\right| > \bar{\tau}_L$ and $\left|\bar{\tau}_b\right| < \bar{\tau}_L$. The velocity distribution across the film that exists in this zone is shown in figure 2(a). Slippage occurs at the top surface so that the velocity at the fluid-solid boundary is denoted by $\tilde{u}_a$. This implies that in this zone the velocity, the velocity gradient, and the shear stresses can be directly obtained from equations (2) to (5) with the substitution for u_a with $\tilde{u}_a$, the slip velocity. Making use of the non-Newtonian model discussed earlier leads to the observation that, since $\bar{\tau}_a > \bar{\tau}_L$, then $\left|\tau_a\right|$ is set equal to τ_L. Solving for this slip velocity at surface a, we get

$$\tilde{u}_a = u_b + \frac{\tau_L h}{\eta} - \frac{h^2}{2\eta} \frac{dp}{dx}$$ (13)

Making use of this equation, we can write the dimensionless velocity, velocity gradient, and shear stress at the bottom surface as

$$\hat{U} = \frac{H^2 Z(Z-2)}{4\bar{\eta}U} \sqrt{\frac{\pi}{2W}} \frac{dP}{dX} + 1 - U^* + \frac{\bar{\tau}_L H Z}{\bar{\eta}U} \tag{14}$$

$$\frac{d\bar{u}}{dZ} = \frac{H^2(Z-1)}{2\bar{\eta}U} \sqrt{\frac{\pi}{2W}} \frac{dP}{dX} + \frac{\bar{\tau}_L H}{\bar{\eta}U} \tag{15}$$

$$\bar{\tau}_b = \bar{\tau}_L - \frac{H}{2} \sqrt{\frac{\pi}{2W}} \frac{dP}{dX} \tag{16}$$

The dimensionless mass flow rate per unit length and the pressure equation for this zone can be written as

$$Q = \frac{q}{\rho_0 u_s R} = \bar{\rho}H \left(1 - U^* + \frac{\bar{\tau}_L H}{2\bar{\eta}U} - \frac{H^2}{6\bar{\eta}U} \sqrt{\frac{\pi}{2W}} \frac{dP}{dX} \right) \tag{17}$$

$$\left(\frac{d}{dX} \frac{\bar{\rho}H^3}{\bar{\eta}} \frac{dP}{dX} \right) = 6U \sqrt{\frac{2W}{\pi}} \left[(1 - U^*)\frac{d}{dX}(\bar{\rho}H) + \frac{1}{2U} \frac{d}{dX}\left(\frac{\bar{\rho}H^2 \bar{\tau}_L}{\bar{\eta}}\right) \right] \tag{18}$$

The nonunity terms in parentheses in equation (17) are the Poiseuille terms. Equation (18) is referred to as the pressure equation but also can be viewed as the Reynolds equation for a non-Newtonian fluid when conditions in zone 1 prevail.

Zone 2

The Newtonian model for zone 2 gives $\bar{\tau}_a < \bar{\tau}_L$ and $\bar{\tau}_b > \bar{\tau}_L$.

The velocity distribution across the film that exists in this zone is shown in figure 2(b). Slippage occurs at the bottom surface (slower moving surface) so that the velocity at the fluid-solid boundary is denoted by

11

$\tilde{u}_b$. This implies that in this zone the velocity, the velocity gradient, and the shear stresses can be written directly from equations (2) to (5) with the substitution for u_b with $\tilde{u}_b$. Since the Newtonian model gives $\bar{\tau}_b > \bar{\tau}_L$, the shear stress at surface b is set equal to $\bar{\tau}_L$. Solving for the slip velocity at surface b, we get

$$\tilde{u}_b = u_a - \frac{\bar{\tau}_L h}{\eta} - \frac{h^2}{2\eta} \frac{dp}{dx} \tag{19}$$

Making use of this equation, we can write the dimensionless velocity, velocity gradient, and shear stress at the top surface as

$$\hat{U} = \frac{H^2(Z^2 - 1)}{4\bar{\eta}U} \sqrt{\frac{\bar{\tau}}{2W}} \frac{dP}{dX} + 1 + U^* - \frac{\bar{\tau}_L(1 - Z)H}{\bar{\eta}U} \tag{20}$$

$$\frac{d\hat{U}}{dZ} = \frac{ZH^2}{2\bar{\eta}U} \sqrt{\frac{\bar{\tau}}{2W}} \frac{dP}{dX} + \frac{\bar{\tau}_L H}{\bar{\eta}U} \tag{21}$$

$$\bar{\tau}_a = \bar{\tau}_L + \frac{H}{2} \sqrt{\frac{\bar{\tau}}{2W}} \frac{dP}{dX} \tag{22}$$

Note that, in order to be in zone 2, $|\bar{\tau}_a| < \bar{\tau}_L$. From equation (22) we observe that this is only possible if dP/dX is negative. Likewise, in zone 1, $|\bar{\tau}_b| < \bar{\tau}_L$. From equation (16) we observe that this is only possible if dP/dX is positive.

The dimensionless mass flow rate per unit length and the appropriate pressure equation for this zone can be written as

$$Q = \bar{\rho}H \left(1 + U^* - \frac{\bar{\tau}_L H}{2\bar{\eta}U} - \frac{H^2}{6\bar{\eta}U} \sqrt{\frac{\bar{\tau}}{2W}} \frac{dP}{dX} \right) \tag{23}$$

$$\frac{d}{dX}\left(\frac{\bar{\rho}H^3}{\bar{\eta}}\frac{dP}{dX}\right) = 6U\sqrt{\frac{2W}{\pi}}\left[(1 + U^*)\frac{d}{dX}(\bar{\rho}H) - \frac{1}{2U}\frac{d}{dX}\left(\frac{\bar{\rho}\,\bar{\tau}_L H^2}{\bar{\eta}}\right)\right] \quad (24)$$

The nonunity terms in the parentheses in equation (23) are the Poiseuille terms.

Zone 3

The Newtonian model for zone 3 gives $\bar{\tau}_a > \bar{\tau}_L$ and equation (16) gives $\bar{\tau}_b \leq -\bar{\tau}_L$. Figure 2(a) shows the velocity distribution across the lubricant film. Slippage occurs at both the top and bottom surfaces, and the slip velocity is less than the velocity of the slow surface (surface b). In this zone the velocity, the velocity gradient, and the shear stresses can be written directly from equations (2) to (5) with the substitution for u_a with $\tilde{u}_a$ and u_b with $\tilde{u}_b$. Since the Newtonian model gives $\bar{\tau}_a > \bar{\tau}_L$, the shear stress at the top surface, surface a, is set equal to $\bar{\tau}_L$ and since equation (16) gives $\bar{\tau}_b \leq -\bar{\tau}_L$, the shear stress at surface b is set equal to $-\bar{\tau}_L$. From these equations we find that $\tilde{u}_a = \tilde{u}_b$. The dimensionless velocity gradient can be written as

$$\hat{U} = \frac{H(Z^2 - Z)\bar{\tau}_L}{\bar{\eta}U} + \frac{\tilde{u}_a}{u_s} \quad (25)$$

$$\frac{d\hat{U}}{dZ} = \frac{H\bar{\tau}_L(2Z - 1)}{\bar{\eta}U} \quad (26)$$

The dimensionless mass flow rate per unit length and the appropriate pressure equation can be written as

$$Q = \bar{\rho}H\left(1 - \frac{u_s - \tilde{u}_a}{u_s} - \frac{H\bar{\tau}_L}{6\bar{\eta}U}\right) \quad (27)$$

$$\frac{dP}{dX} = 4\sqrt{\frac{2W}{\pi}}\frac{\bar{\tau}_L}{H} \quad (28)$$

The nonunity terms in parentheses in equation (27) are the Poiseuille terms.

13

The Newtonian model for zone 4 gives $\bar{\tau}_b > \bar{\tau}_L$ and equation (22) gives $\bar{\tau}_a \leq -\bar{\tau}_L$. Figure 2(b) shows the velocity distribution across the lubricant film. Slippage occurs at both the top and bottom surfaces. The difference between zone 3 and zone 4 is that in zone 3 the slip velocity is less than the slower surface velocity and in zone 4 the slip velocity is greater than the faster surface velocity. In zone 4 the velocity, the velocity gradient, and shear stresses can be written directly from equations (2) to (5) with

the substitution for u_a with $\tilde{u}_a$ and u_b with $\tilde{u}_b$. Since equation (22) gives $\bar{\tau}_a \leq -\bar{\tau}_L$, the shear stress at surface a is set equal to $-\bar{\tau}_L$; and since the Newtonian model gives $\bar{\tau}_b > \bar{\tau}_L$, the shear stress at surface b is set equal to $\bar{\tau}_L$. The dimensionless velocity, velocity gradient, mass flow, and pressure can be directly written from the equations developed in zone 3 (eqs. (25) to (28)) if $\overset{-}{\tau}_L$ is substituted for $\bar{\tau}_L$. Note that in order to be in zone 3 from equation (28), the pressure gradient must be positive; and in order to be in zone 4, the pressure gradient must be negative.

Density, Viscosity, and Film Shape Equations

The equations that define velocity, velocity gradient, shear stress, flow, and pressure for the five zones have been defined. Before proceeding, however, the dimensionless density, viscosity, and film shape need to be expressed. For a comparable change in pressure the density change is small as compared with the viscosity change. However, very high pressure exists in elastohydrodynamic films, and the liquid can no longer be considered as an incompressible medium. From Dowson and Higginson (1966) the dimensionless density can be written as

$$\bar{\rho} = \frac{\rho}{\rho_0} = 1 + \frac{0.6E'P}{1 + 1.7E'P} \tag{29}$$

where E' is expressed in gigapascals.

The effects of pressure on viscosity can be written as

$$\bar{\eta} = \frac{\eta}{\eta_0} = e^{\alpha P} = e^{GP} \qquad \qquad (30)$$

where

α pressure-viscosity coefficient of lubricant, m^2/N

η_0 viscosity at atmospheric conditions, $N\ s/m^2$

The film shape equation can be written from Hamrock and Jacobson (1982) in dimensionless form as

$$H_k = \frac{h}{R} = H_0 + \frac{1}{R}\left[\frac{x^2}{2}\left(\frac{b^2}{R}\right) + \frac{2}{\pi}\sum_i P_i D_j\right] \qquad (31)$$

where

$$j = k - i + 1$$

$$D = b[(\bar{X} - B)\ln(\bar{X} - B)^2 - (\bar{X} + B)\ln(\bar{X} + B)^2 + 4B(1 - \ln b)]$$

and

b   semiwidth of the Hertzian contact, $R\sqrt{8W/\pi}$

B $1/n$

n   number of nodes in semiaxis of contact

The last term in equation (31) represents the elastic deformation at a point $\bar{x}$ due to the contribution of various rectangular areas of uniform pressure in the conjunction.

Having defined density, viscosity, and film shape, we can return to the solution of the mass flow and pressure equations for the five zones. The first step is to rewrite these equations by finite difference approximations which rely on the fact that a function can be represented with sufficient accuracy over a small range by a quadratic expression. Standard finite central-difference representation was used, and a procedure similar to that given in Hamrock and Jacobson (1982) was followed. Figure 3 shows the flow chart of the pressure loop in the computer program used to evaluate the mass flow and pres-

sure from the inlet to the outlet. In this figure the procedure used in evaluating zone 0, the Newtonian model, was quite similar to that used in Hamrock and Jacobson (1982). A similar procedure was used in evaluating the other zones.

Having defined the pressure from the inlet to the outlet for the non-Newtonian fluid model, we can evaluate the force components, the shear forces, and the coefficient of friction. The relevant expressions are presented in Hamrock and Jacobson (1982) and are not repeated here.

RESULTS

Dimensionless Grouping

From the variables of the numerical analysis the following dimensionless groups can be defined:

(1) Dimensionless film thickness: $H = \dfrac{h}{R}$

(2) Dimensionless load parameter: $W = \dfrac{w_z}{E'R}$

(3) Dimensionless speed parameter: $U = \dfrac{\eta_0 u_s}{E'R}$

(4) Dimensionless materials parameter: $G = \alpha E'$

(5) Dimensionless sliding velocity: $U^* = \dfrac{u_d}{u_s} = \dfrac{u_a - u_b}{u_a + u_b}$

(6) Limiting-shear-strength proportionality constant: γ

The first four groups were used for the Newtonian fluid analysis in Hamrock and Jacobson (1982). The dimensionless film thickness for a rectangular contact with a non-Newtonian fluid can be written as

$$H_{min} = H_{min,N} f(U^*, \gamma, U, W, G) \tag{32}$$

16

The dimensionless minimum film thickness for a Newtonian fluid as obtained from Hamrock and Jacobson (1982) can be written as

$$H_{min,N} = 3.07 \ U^{0.71} G^{0.57} W^{-0.11} \tag{33}$$

In the present analysis the dimensionless parameters U^* and γ were varied and the effect on the minimum film thickness was studied.

Pressure and Film Profiles

Representative variations of dimensionless pressure, film thickness, shear stress distribution, and mass flow are shown in figures 4 to 6. In these figures the inlet region is to the left and the outlet region is to the right. Figure 4 shows the variation of dimensionless pressure and film thickness on the X axis for four dimensionless sliding velocities. The Hertzian pressure is also shown in this figure. The characteristic pressure spike is clearly evident for each dimensionless sliding velocity, but the spike diminishes as the sliding velocity increases. Also clearly evident for each sliding velocity is the parallel film shape through the central part of the contact, with a minimum film thickness occurring near the outlet of the contact. As the dimensionless sliding velocity increases, the central parallel film thickness decreases more than the minimum film thickness decreases. As a result the nip decreases with increasing sliding velocity, where the nip is that portion of the film shape from the tip of the pressure spike to the outlet of the conjunction.

Variation of Shear Stress

The shear stress ratio is defined as the shear stress divided by the limiting shear stress. Variations of the shear stress ratio at the top

$(\bar{\tau}_a)$ and bottom $(\bar{\tau}_b)$ surfaces on the X axis are shown in figure 5 for the four dimensionless sliding velocities given in figure 4. Recall that the top surface (surface a) is moving with a greater velocity than the bottom surface (surface b). For the condition of no sliding ($U^* = 0$) zone 0, the Newtonian model, is valid for the entire conjunction, and the shear stress ratio of the top surface $\hat{\tau}_a$ is symmetrical to the shear stress ratio of the bottom surface $\hat{\tau}_b$ about the zero axis. From equations (9) and (10) this effect is clearly evident. In these equations the first term on the right is set equal to zero since $U^* = 0$, and the only remaining effect is the pressure gradient. There is a difference in sign for the different surfaces. For sliding velocities U^* of 0.01 and 0.02 zones 1 and 2 appear at the tip of the spike and zone 0, the Newtonian model, occurs elsewhere. For $U^* = 0.04$ the zone allocation going from the inlet to the outlet (left to right) is zone 0 to zone 1, to zone 2, back to zone 0; then in the spike zones 1 and 2 reoccur. Zones 3 and 4 do not occur in the final results for figure 5, but these zones are used to derive a converged solution. For the higher load cases, however, zones 3 and 4 do appear in the final converged solution.

The shear stress ratio in the inlet up to the beginning of the Hertzian contact is quite similar for all four sliding velocities. From the beginning of the Hertzian contact to the tip of the pressure spike there is substantial change in the shear stress ratio from $U^* = 0$ to $U^* = 0.04$. As the dimensionless sliding velocity increases, the shear stress ratio increases until for $U^* = 0.04$ there is a large region where the shear stress is equal to the limiting shear stress. From figure 4 we found that the pressure spike decreases with increasing sliding velocity. The result of this is clearly

18

evident in figure 5, where from the tip of the pressure spike to the exit the shear stress ratio at the top surface $\hat{\tau}_a$ becomes less negative with increasing dimensionless sliding velocity. The effect of using the non-Newtonian model is quite significant for the largest dimensionless sliding velocity in figure 5.

Flow Results

A typical variation of dimensionless flow and the Poiseuille flow terms on the X axis is shown in figure 6. Since there was very little difference for the various sliding velocities, a typical result is shown. Equations (11), (17), (23), and (27) define the dimensionless mass flow rate for the five zones considered. The Poiseuille flow term in these equations is the term or terms other than the unity in the parentheses on the right side of these equations. From figure 6 we find the flow to be constant throughout the contact. Great care was taken to assure that this was maintained for all the results presented. As in the authors' earlier publication (Hamrock and Jacobson, 1982) slight adjustments in pressure profile were necessary in the inlet region to assure a constant flow. The Poiseuille term approaches unity at the inlet, is near zero from the beginning of the Hertzian contact to the location of the pressure spike, and is negative from the pressure spike to the outlet.

Effect on Coefficient of Friction

Figure 7 shows the effect of dimensionless sliding velocity U^* on the coefficient of friction μ for three dimensionless loads. For higher loads the asymptotic value of the coefficient of friction is reached at lower dimensionless sliding velocities. The dimensionless sliding velocity given in this

19

figure can be equated to the conventional sliding velocity in percent by multiplying the value of $U*$ by 200. For example $U* = 0.03$ corresponds to a conventional 6 percent sliding speed. The results for a Newtonian fluid are shown in this figure with dashed lines. The asymptotic value of the coefficient of friction is between 0.07 and 0.08 for a limiting-shear-strength proportionality constant γ of 0.07.

Influence of Sliding Velocity

Cases 1 to 6 of table I show the effect of six values of dimensionless sliding velocity $U*$ on dimensionless minimum film thickness for constant values of the other dimensionless parameters. From these results it is observed that as the sliding velocity is increased the minimum film thickness decreases. However, the influence of sliding velocity was found to be not simply a function of minimum film thickness but had to be coupled with the dimensionless speed, load, and materials parameters. Table I also shows these results. The resulting relationship is

$$\frac{\overline{H}_{min}}{\overline{H}_{min,N}} = 1 - 4.07 \times 10^{-9} (U*)^{0.60} U^{0.23} (WG^2)^{3.85} \tag{34}$$

The influence of the maximum pressure is represented in this equation by the grouping WG^2. The coefficient of determination ϵ was also calculated for these results. The value of ϵ reflects the fit of the data to the resulting equation: unity representing a perfect fit, and zero the worse possible fit. The coefficient of determination for these results was 0.9990, which is excellent.

Influence of Limiting Shear Strength

Cases 9 and 10 of table I show the influence of the limiting-shear-strength proportionality constant γ on dimensionless film thickness for constant values of the other dimensionless parameters. From these three cases covering the complete range of natural and synthetic lubricating fluids, the following relationship was found:

$$\frac{\overline{H}_{min}}{\overline{H}_{min,N}} = 1 + 2.06(\gamma - 0.07) \tag{35}$$

The coefficient of determination was found to be 0.9995, which is excellent.

Minimum Film Thickness

The proportionality equations (34) and (35) have established how the non-Newtonian fluid rheological model affects the minimum film thickness for low sliding speeds. At high sliding speeds the oil film thickness is mainly governed by the velocity of the slower surface. The reason for this is that the shear strength is reached at the faster surface and the oil velocity is given by the slower surface. This phenomenon occurs in the inlet of the conjunction. The high-sliding-speed cases have not been numerically computed because of numerical instability. For the film thickness equation to accommodate these high-sliding-speed situations, the film thickness equation had to be modified as indicated below.

$$\overline{H}_{min} = \overline{H}_{min,N} \left\{ \exp\left[-4.09 \times 10^{-9}(U^*)^{0.60} U^{0.23}(WG^2)^{3.85} + 2.06(\gamma - 0.07) \right] \right.$$
$$\left. + U^*_f{}^{0.71}(1 - U^*)^{0.71} \right. \tag{36}$$

This dimensionless minimum-isothermal-film thickness formula is for fully flooded rectangular lubricated contacts incorporating non-Newtonian rheological effects. Asymptotically this equation gives the minimum film thickness at high pressures (>1 GPa as equal to zero if one of the surfaces is stationary.

Table I gives the fourteen cases used in evaluating equation (36). In this table H_{min}, the minimum film thickness obtained from equation (36), corresponds to the minimum film thickness obtained from the non-Newtonian elastohydrodynamic lubrication theory developed earlier. The minimum-film-thickness equation obtained from Hamrock and Jacobson (1982) for the Newtonian elastohydrodynamically lubricated rectangular contact is denoted by $H_{min,N}$ and is given in equation (33). The ratios $H_{min}/\overline{H}_{min,N}$ and $\overline{H}_{min}/\overline{H}_{min,N}$ are also given in table I. The percentage difference between H_{min} and $\overline{H}_{min}$ is expressed by V_1, which is defined as

$$V_1 = \left(\frac{\overline{H}_{min} - H_{min}}{H_{min}} \right) 100 \qquad (37)$$

In table I the values of V_1 are within ±1.0 percent.

Coefficient of Friction

OF POOR QUALITY

The values of the coefficient of friction for the 14 cases studied are given in table I. Making use of these results, we can write an approximate formula for the coefficient of friction as

$$\overline{\mu}_1 = 0.67 \times 10^{-6} (U^*)^{0.81} U^{0.26} (WG^2)^{3.32} \qquad \text{when} \quad \overline{\mu}_1 \leq 0.8 \, \gamma \qquad (38)$$

If the coefficient of friction $\overline{\mu}_1$ is greater than 0.8 γ, the following approximate expression should be used:

$$\overline{\mu} = 0.80 \, \gamma + 0.021 \tanh \left[\frac{\overline{\mu}_1}{\gamma} - 0.80 \right] \qquad \text{when} \quad \overline{\mu}_1 > 0.8 \, \gamma \qquad (39)$$

22

This coefficient of friction is mainly determined by the shear strength of the lubricant. The percentage difference between μ and $\bar{\mu}$ is expressed by V_3, where

$$V_3 = \left(\frac{\bar{\mu} - \mu}{\mu} \, 100 \right) \tag{40}$$

In table II the values of V_3 are within ± 9 percent. Equation (39) was derived from eight calculations of the coefficient of friction with sliding velocities up to 20 percent and different γ values. In these calculations the pressure distributions from the lower sliding velocities were used.

CONCLUSIONS

A procedure for the numerical solution of the complete elastohydrodynamic lubrication of rectangular contacts incorporating a non-Newtonian rheological model is outlined. The approach uses a Newtonian model as long as the shear stress is less than the limiting shear stress. If the shear stress exceeds the limiting shear stress, the shear stress is set equal to the limiting shear stress. The limiting shear stress is expressed as a semiempirical linear function of pressure. The numerical solution therefore requires the coupled solution of the pressure, film shape, and fluid rheology equations from the inlet to the outlet without making any assumptions other than neglecting side leakage.

By using the procedures outline in the analysis the influence of the dimensionless speed U, load W, and materials G parameters, dimensionless sliding velocity U*, and limiting shear-strength proportionality constant γ on minimum film thickness H_{min} has been investigated. Fourteen cases were used to generate the minimum film-thickness equation for an elastohydro-dynamically lubricated rectangular contact incorporating a non-Newtonian rheological model:

$$\overline{H}_{min} = \overline{H}_{min,N} \left\{ \exp\left[-4.07 \times 10^{-9} (U*)^{0.60} U^{0.23} (WG^2)^{3.85} + 2.06(\gamma - 0.07)\right] + U* \right\}^{0.71} (1 - U*)^{0.71}$$

The minimum-film-thickness equation obtained for an elastohydrodynamically lubricated rectangular contact incorporating a Newtonian fluid rheology model was developed by the authors in an earlier publication (Hamrock and Jacobson, 1982) where

$$\overline{H}_{min,N} = 3.07 \ U^{0.71} G^{0.57} W^{-0.11}$$

Besides the dimensionless film thickness formula, formulas for the coefficient of friction were developed.

$$\overline{\mu}_1 = 0.67 \times 10^{-6} (U*)^{0.81} U^{0.26} (WG^2)^{3.32} \qquad \text{for } \overline{\mu}_1 \leq 0.8 \ \gamma$$

$$\overline{\mu} = 0.080 \ \gamma + 0.021 \ \tanh\left[\frac{\overline{\mu}_1}{\gamma} - 0.80\right] \qquad \text{for } \mu_1 > 0.8 \ \gamma$$

Computer plots are presented that indicate in detail pressure distribution, film shape, shear stresses at the surface, and mass flow throughout the conjunction. The characteristic pressure spike is clearly evident for each of the sliding velocities, but the spike diminishes as the sliding velocity increases. Also clearly evident in the computer plots is the parallel film shape through the central part of the contact, with a minimum occurring near the outlet of the contact. The central parallel film thickness decreases more than the minimum film thickness decreases with increasing sliding velocity. The result of this is that the nip decreases with increasing sliding velocity, where the nip is that portion of the film shape from the location of the pressure spike to the outlet of the conjunction. The computer plots of the shear stress at the surfaces indicate that as the sliding velocity increases these stresses approach or equal the limiting shear stress. A sample computer plot of the

flow shows that it is constant throughout the conjunction. The effect of sliding velocity on coefficient of friction for various loads indicates that as the load increases, the limiting value of the coefficient of fricton is reached for a much lower value of sliding velocity.

National Aeronautics and Space Administration

Lewis Research Center

Cleveland, Ohio 44135, December 23, 1982

REFERENCES

Bair, S. and Winer, W. O. (1979) "Shear Strength Measurements of Lubricants at High Pressure", J. Lubr. Technol., Vol. 101 (3), pp. 251-257.

Dowson, D. and Higginson, G. R. (1966), Elastohydrodynamic Lubrication, The Fundamentals of Roller and Gear Lubrication, Pergamon, Oxford.

Gacim, B. and Winer, W.O. (1981) "A Film Thickness Analysis for Line Contacts under Pure Rolling Conditions with a Non-Newtonian Rheological Model," J. Lubr. Technol., vol. 103(2), pp. 305-316.

Hamrock, B. J. and Dowson, D. (1981) Ball Bearing Lubrication - The Elastohydrodynamics of Elliptical Contacts, John Wiley & Sons, New York.

Hamrock, B. J. and Jacobson, B. O. (1982) "Elastohydrodynamic Lubrication of Rectangular Contacts", NASA TP-2111, 1983.

Jacobson, B. O. (1970) "On the Lubrication of Heavily Loaded Spherical Surfaces Considering Surface Deformation and Solidification of the Lubricant", Acta Polytech. Scand., Mech. Eng. Ser. No. 54.

Tevaarwerk, J.L. (1976) The Shear of Elastohydrodynamic Oil Films, Ph.D. thesis, Cambridge, England.

TABLE I. – EFFECT OF DIMENSIONLESS PARAMETERS ON MINIMUM FILM THICKNESS

Case	Dimensionless load parameter, W	Dimensionless speed parameter, U	Dimensionless materials parameter, G	Dimensionless sliding velocity, u_a	Limiting-shear-strength proportionality constant, γ	Dimensionless minimum film thickness, H_{min}	$\dfrac{H_{min}}{H_{min,N}}$	$\dfrac{\bar{H}_{min}}{H_{min,N}}$	Difference, V_1, percent	Coefficient of friction, μ	Coefficient of friction from least-squares fit, $\bar{\mu}$	Difference, V_3, percent
1	2.0478×10^{-5}	1.0000×10^{-11}	5000	0	0.07	19.524×10^{-6}	1.000	1.000	0	0.00054	————	————
2				.005		19.300	.989	.990	.15	.01227	0.01250	1.87
3				.010		19.284	.988	.986	– .23	.02015	.02191	8.73
4				.020		19.260	.986	.978	– .74	.03613	.03842	6.34
5				.030		18.976	.972	.972	0	.05309	.05336	.51
6	1.6382			.040		18.687	.957	.967	1.09	.06316	.06403	1.38
7	1.6382			0		20.327	1.000	1.000	0	.00081	————	————
8	2.0478			.040	.04	20.133	.990	.986	– .47	.03479	.03210	–7.73
9	2.0478			.020	.10	18.448	.945	.935	– .82	.03618	.03534	–2.32
10	4.0094	5.5975	3591.1	.020	.07	20.134	1.031	1.021	– .93	.03592	.03842	6.96
11	4.0094	5.5975	3591.1	0		52.502	1.000	1.000	0	.00202	————	————
12	3.0000	1.0000	5000	.014		51.068	.973	.973	0	.04678	.04655	– .49
13	3.0000	1.0000	5000	0		19.055	1.000	1.000	0	.00087	————	————
14				.005		18.442	.968	.958	– .89	.04744	.04441	–6.39

TABLE II. - EFFECT OF DIMENSIONLESS PARAMETERS ON
DIMENSIONLESS CENTER OF PRESSURE

Case	Dimensionless center of pressure, X_{cp}	Dimensionless center of pressure from least-squares fit, $\bar{X}_{cp}$	Difference, V_2, percent	Coefficient of friction, μ	Coefficient of friction from least-squares fit, $\bar{\mu}$	Difference, V_3, percent
1	−0.1487	−0.1487	0	0.00054	------	------
2	− .1480	− .1469	− .71	.01227	0.01250	1.87
3	− .1430	− .1452	1.52	.02015	.02191	8.73
4	− .1384	− .l᠎᠎	2.35	.03613	.03842	6.34
5	− .1361	− .1᠎᠎l	1.49	.05309	.05336	.51
6	− .1346	− .1346	0	.06316	.06403	1.38
7	− .1912	− .1912	0	.00081	------	------
8	− .1845	− .1730	− 9.48	.03479	.03210	−7.73
9	− .1360	− .1417	4.16	.03618	.03534	−2.32
10	− .1383	− .1417	2.46	.03592	.03842	6.96
11	− .1810	− .1810	0	.00202	------	------
12	− .1841	− .1753	−4.79	.04678	.04655	− .49
13	− .0971	− .0971	0	.00087	------	------
14	− .0973	− .0960	−1.34	.04744	.04441	−6.39
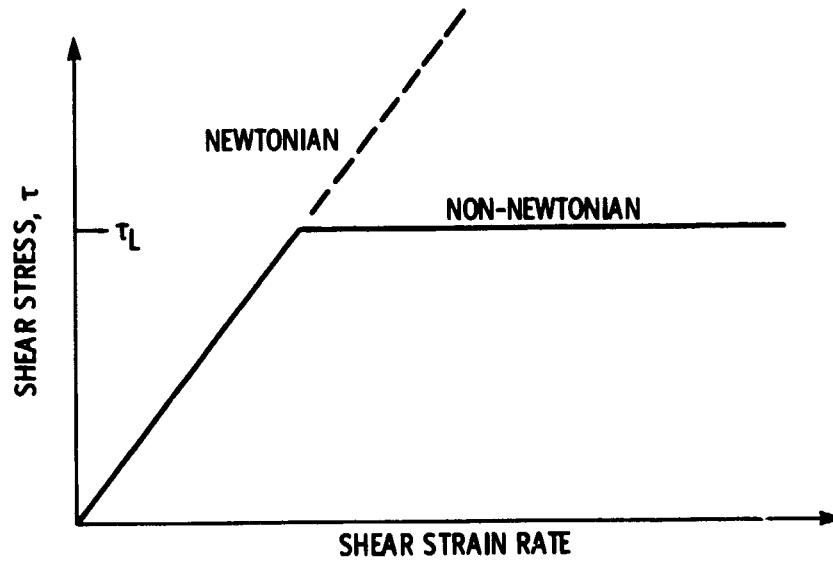
Figure 1 - Lubricant model.
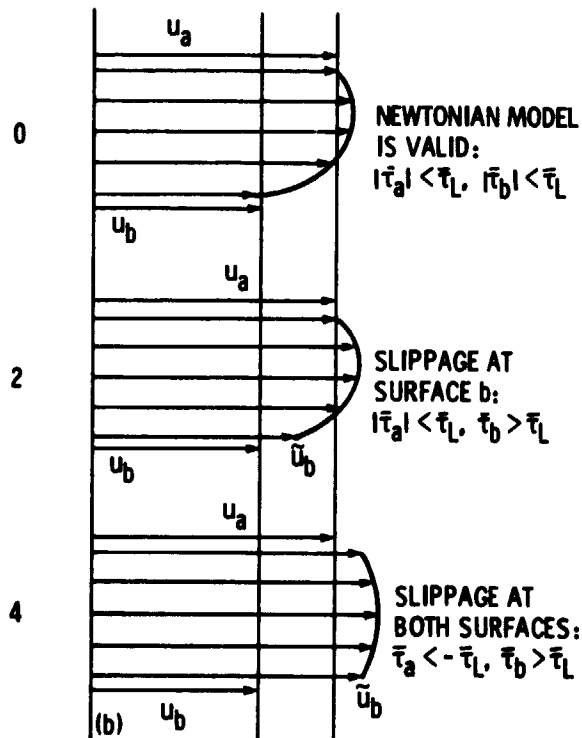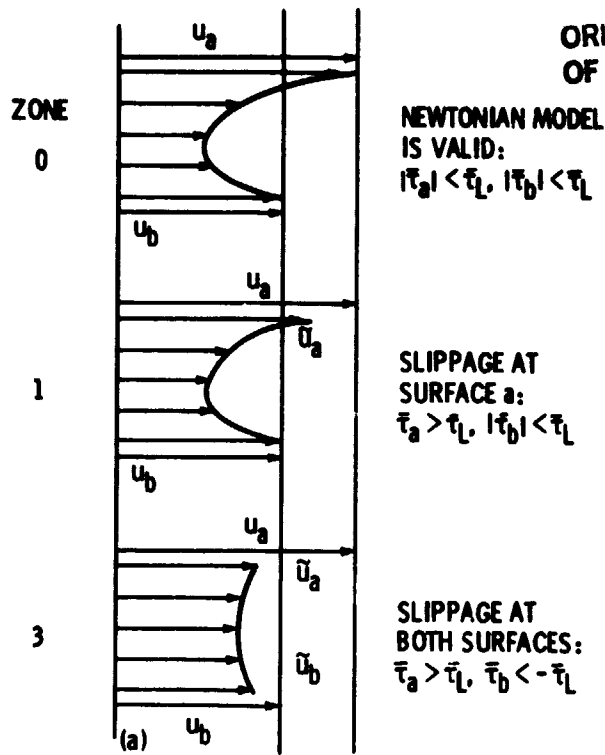
Figure 2. – Velocity distributions in the different lubri-
cating zones.

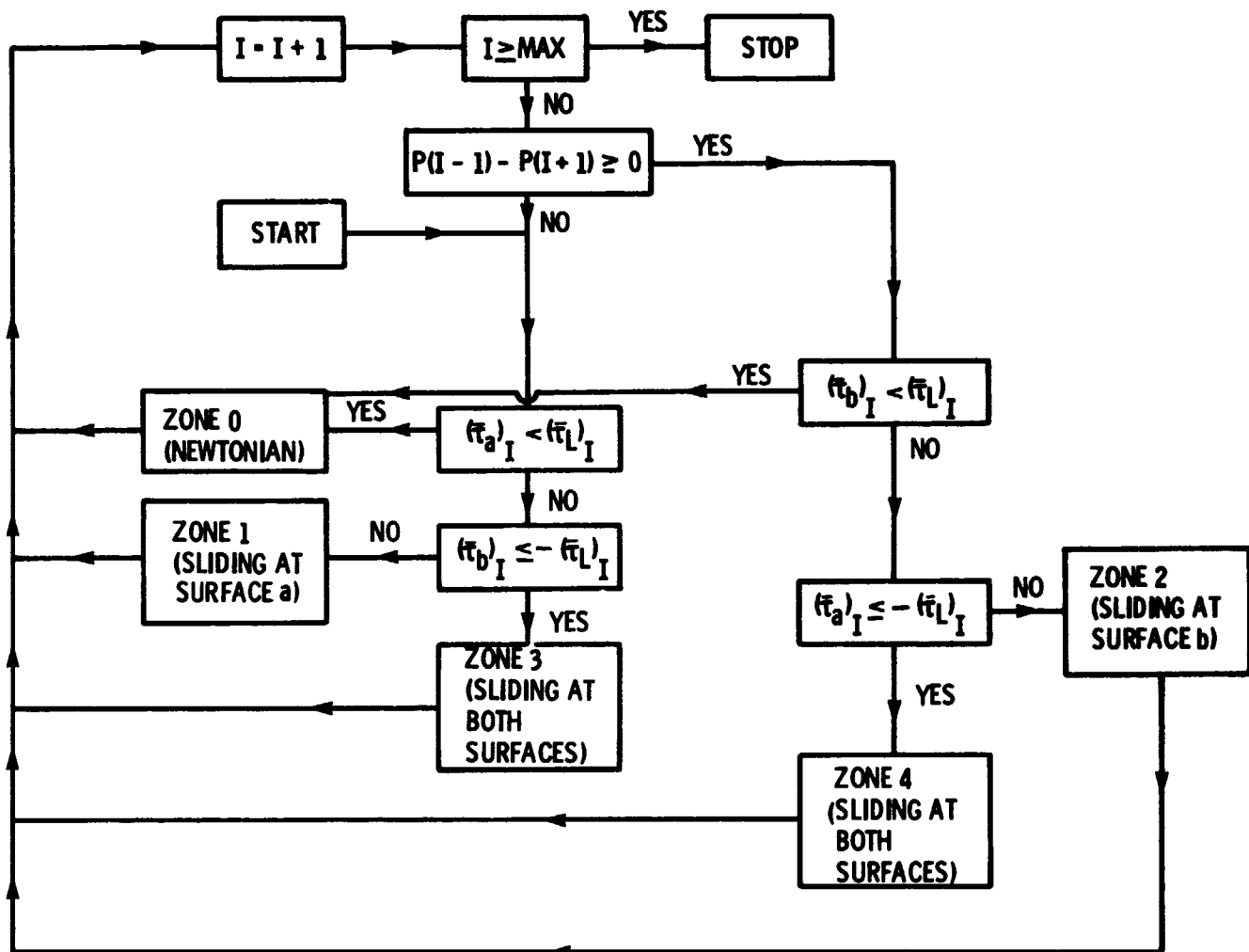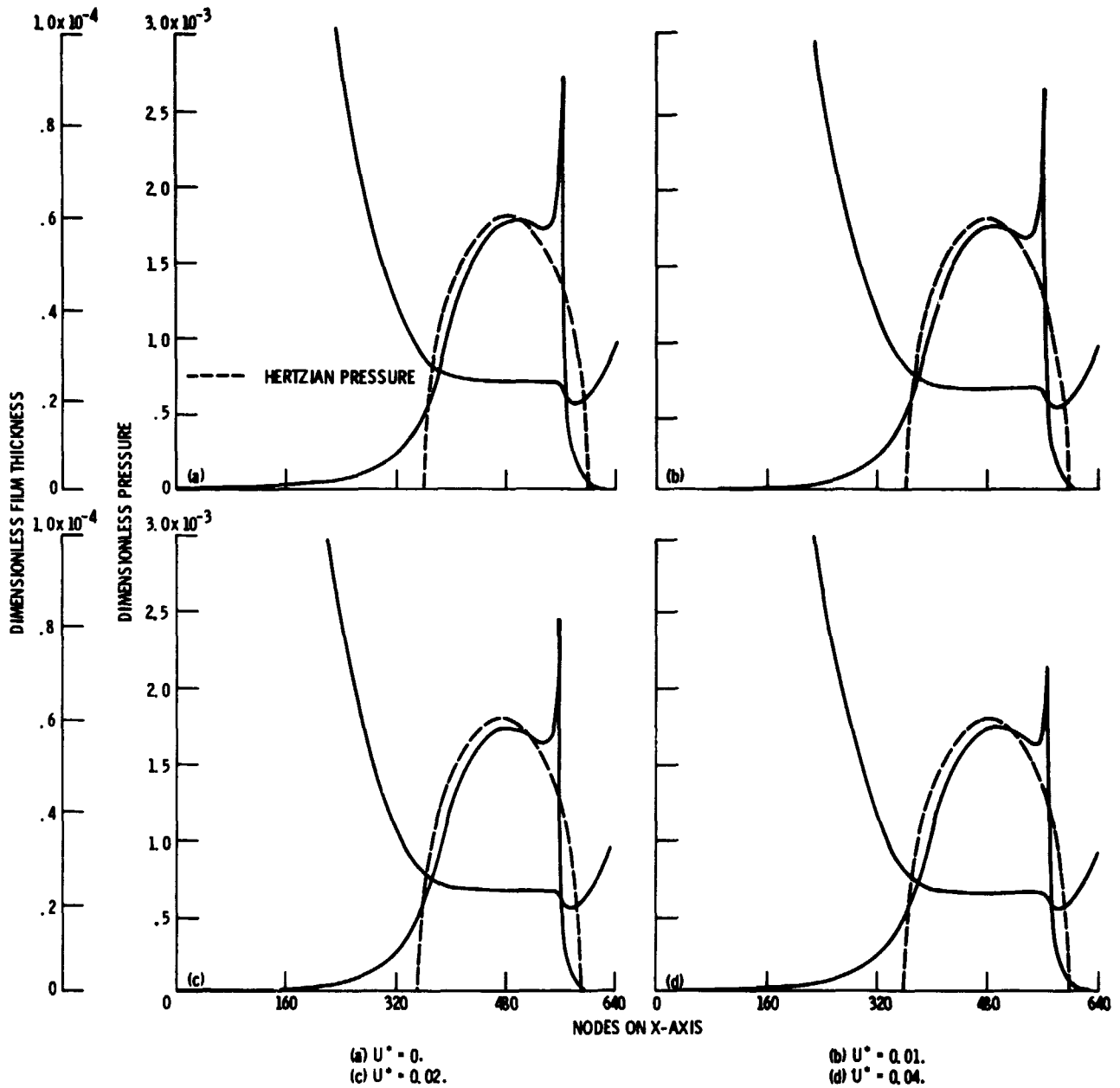Figure 3. - Flow diagram.

Figure 4. - Pressure distributions and film shapes for different sliding velocities U*. Dimensionless load parameter W, 2.0478 x 10^{-5}; dimensionless speed parameter U, 10^{-11}; dimensionless materials parameter G, 5000; limiting-shear-strength proportionality constant γ, 0.07.
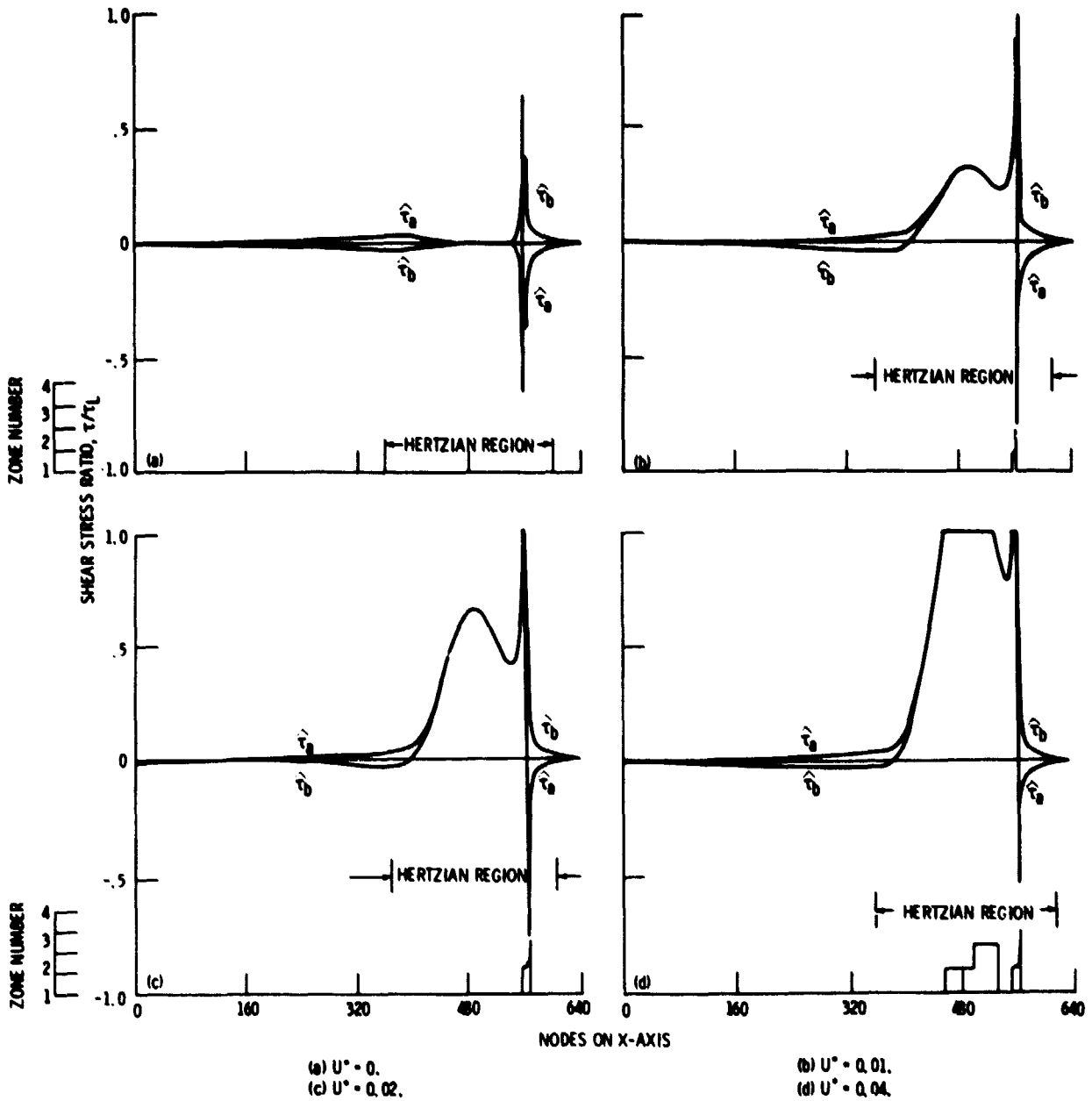
(a) U* = 0.
(c) U* = 0.02.
(b) U* = 0.01.
(d) U* = 0.04.

Figure 5. - Shear stress distributions and lubricating zones for different sliding velocities U*. Dimensionless load parameter W, 2.0478 x 10^-5; dimensionless speed parameter U, 10^-11; dimensionless materials parameter G, 5000; limiting-shear-strength proportionality constant γ, 0.07.
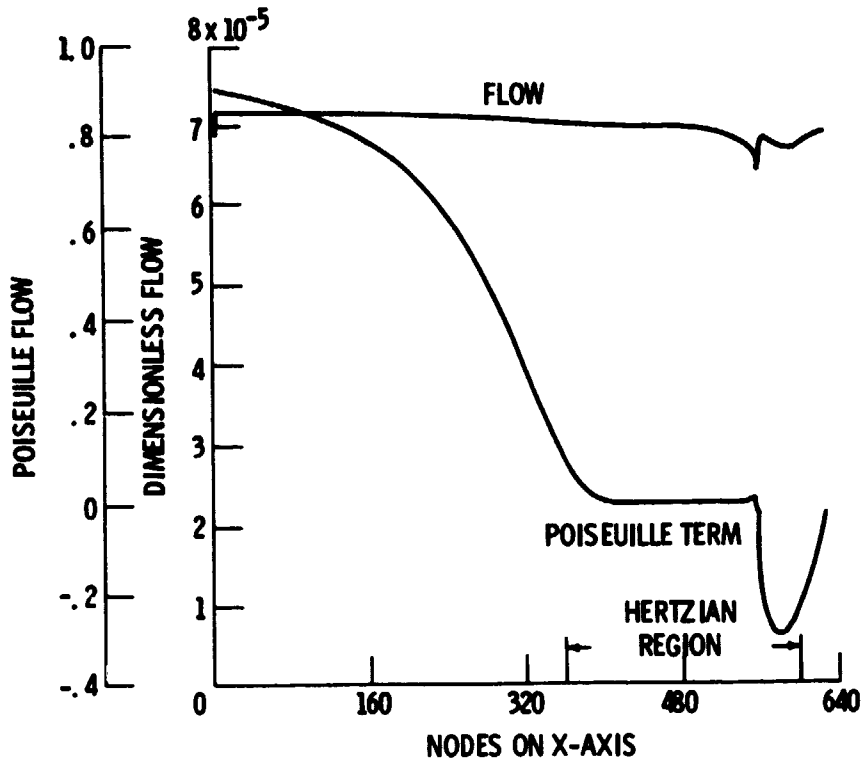
(a) U* = 0.
(c) U* = 0.02.

(b) U* = 0.01.
(d) U* = 0.04.

Figure 6. - Oil flow through contact - total flow and
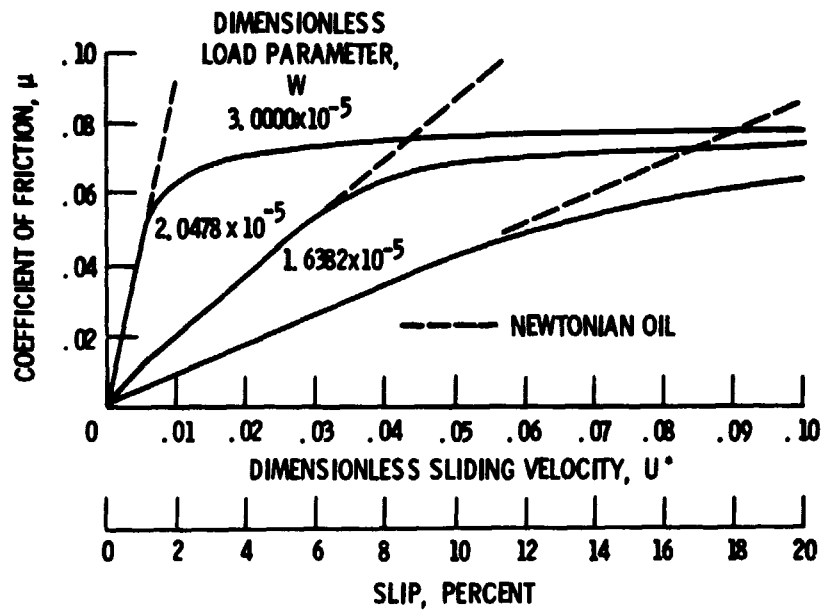Poiseuille term.

Figure 7. - Coefficient of friction as a function of load and dimensionless sliding velocity. Dimensionless speed parameter U, 10^{-11}; dimensionless materials parameter G, 5000; limiting-shear-strength proportionality constant γ, 0.07.